Dramatic Synergy in CoPt Nanocatalysts Stabilized by "Click" Dendrimers for Evolution of Hydrogen from Hydrolysis of Ammonia Borane

Qi Wang, Fangyu Fu, Sha Yang, Marta Martinez Moro, Maria de Los Angeles Ramirez, Sergio Moya, Lionel Salmon, Jaime Ruiz, Didier Astruc

Dramatic Synergy in CoPt Nanocatalysts Stabilized by "Click" Dendrimers for Evolution of Hydrogen from Hydrolysis of Ammonia Borane

SCHOLARONE™
Manuscripts

Dramatic Synergy in CoPt Nanocatalysts Stabilized by "Click" Dendrimers for Evolution of Hydrogen from Hydrolysis of Ammonia Borane

Qi Wang,[a] Fangyu Fu,[a] Sha Yang, [b] Marta Martinez Moro,[c] Maria de los Angeles Ramirez,[c] Sergio Moya, [c] Lionel Salmon,[d] Jaime Ruiz,[a] and Didier Astruc[a]*

a ISM, UMR CNRS N° 5255, Univ. Bordeaux, 33405 Talence Cedex, France.

b Department of Chemistry and Centre for Atomic Engineering of Advanced Materials, Anhui Province Key Laboratory of Chemistry for Inorganic/Organic Hybrid Functionalized Materials, Anhui University, Hefei, Anhui 230601, China

c Soft Matter Nanotechnology Lab, CIC biomaGUNE, Paseo Miramón 182. 20014. Donostia-San Sebastián, Gipuzkoa, Spain.

d Laboratoire de Chimie de Coordination, UPR CNRS 8241, 31077 Toulouse Cedex, France

ABSTRACT

Hydrolysis of ammonia-borane (AB) is one of the most convenient sources of H_2 under ambient conditions, but the reaction requires a good catalyst to become efficient. Here this reaction is catalyzed by bimetallic late transition-metal nanoparticles (NPs) stabilized by "click" dendrimers **1** and **2** containing respectively 27 or 81 terminal triethylene glycol termini and 9 or 27 intradendritic 1,2,3-triazole ligands. A remarkable synergy between Pt and Co in the Pt-Co/"click" dendrimer nanocatalyst is disclosed. These Pt-Co/"click" dendrimer catalysts are much more efficient for hydrolysis of AB than either "click" dendrimer-stabilized Co or Pt analogues alone. The best catalyst $Pt_1Co_1/$**1** stabilized by the nona-triazole "click" dendrimer **1** achieves a TOF of 303 $mol_{H2} \cdot mol_{catal.}^{-1} \cdot min^{-1}$ (606 $mol_{H2} \cdot mol_{Pt}^{-1} \cdot min^{-1}$) at $20 \pm 1°C$. In the presence of NaOH, the reactivity is boosted for hydrolysis of AB catalyzed by $Pt_1Co_1/$**1**, and reaches a TOF value of 476.2 $mol_{H2} \cdot mol_{catal.}^{-1} \cdot min^{-1}$ (952.4 $mol_{H2} \cdot mol_{Pt}^{-1} \cdot min^{-1}$), one of the very best results obtained by comparison with the literature. The presence of a percentage of Pt as low as 25% in the CoPt nanoalloy provides a reaction rate higher than with that obtained with the pure Pt NP catalyst alone. The kinetics involves in particular a kinetic isotope effect $k_D/k_H = 2.46$ obtained for the hydrolysis reaction with D_2O, suggesting O-H bond cleavage of water in the rate-determining step. Tandem reactions were conducted for the hydrogenation of styrene with hydrogen generated from the hydrolysis of AB. Performing this tandem reaction with D_2O shows deuteration of the ethylbenzene products confirming O-D cleavage and H/D scrambling on the bimetallic nanoparticle surface. Finally a reaction mechanism is proposed. This dramatic synergy type should also prove useful in a number of other catalytic systems.

KEYWORDS: Synergy; nanocatalyst; cobalt; dendrimer; hydrolysis; ammonia borane

INTRODUCTION

Hydrogen energy is regarded as the most promising clean energy in the 21st century. H_2 production upon hydrolysis of ammonia borane (AB) has attracted increasing attention owing to the high AB hydrogen content (19.6 wt%), low molecular weight (30.87 g·mol^{-1}) and high stability in solution.[1] Duan and Chen recently reported mechanistic studies for the hydrolysis of AB, showing that the reaction produces $NH_4^+B(OH)_4^-$:[2]

$$H_3N·BH_3 + 4\ H_2O \rightarrow NH_4^+B(OH)_4^- + 3\ H_2$$
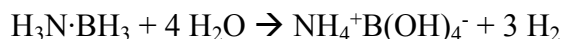
In the past decade, intensive efforts have been devoted to the investigation of potentially efficient and economical catalysts for the hydrolysis of AB.[3,4] Noble-metal nanoparticles (NPs), in particular Pt-based catalysts, have been shown to undergo high hydrogen evolution rates for this reaction.[5] Non-noble-metal NPs catalysts are much less efficient than their noble metal analogues, however.[6] For example, under the same conditions PtNPs and RhNPs showed much higher efficiency than CoNPs and NiNPs for the hydrolysis of AB,[7] but the practical use of precious metals in catalysis is limited owing to their high costs and global scarcities.

Dendrimers have been extensively used as supports and shown to be highly efficient in catalysis,[8] including for the encapsulation or stabilization of transition-metal NP catalysts.[9] Their use to generate hydrogen from hydrogen-rich precursors has been pioneered by Xu's group,[10] but they have very rarely been used for this purpose. Only two reports are known, and they deal with monometallic NPs.[7,10] There is so far no report of dendrimer-stabilized bimetallic nanocatalyst for hydrogen generation. Here we report a series of bimetallic NPs with narrow size distributions stabilized by "click" dendrimers[11] for optimized catalysis of AB hydrolysis using the possible

synergy between the two metals.[12] Two water-soluble arene-centered triethylene glycol (TEG)-terminated "click" dendrimers **1** and **2** of zeroth and first generation containing respectively 27 and 81 TEG tethers are serving as nanoparticle stabilizers (Figure 1). Then homogenerous bimetallic catalysts are prepared by mixing the two precursor metal salts with one of the dendrimers in water, followed by reduction of the mixture of the transition-metal salts by $NaBH_4$. These bimetallic nanocatalysts are characterized by transmission electron microscopy (TEM), high-resolution transmission electron microscopy (HRTEM), high-angle annular dark-field scanning transmission electron microscopy (HADDF-STEM), energy dispersive X-ray spectroscopy (EDS) and X-ray photoelectron spectra (XPS). Among these click-dendrimer templated bimetallic NPs, the nanoalloy Pt_1Co_1/**1** is shown to be the most active and efficient nanocatalyst for AB hydrolysis, achieving a TOF value of 952.4 $mol_{H2} \cdot mol_{Pt}^{-1} \cdot min^{-1}$. The influence of $NaOH^{[13]}$ on the reaction efficiency for various bimetallic NPs is investigated. Kinetic isotope effects (KIEs)[14] using D_2O instead of H_2O and tandem reaction for hydrogenation of styrene are also examined for the mechanistic study of this reaction.

1
2
3
4
5
6
7
8
9
10
11
12
13
14
15
16
17
18
19
20
21
22
23
24
25
26
27
28
29
30
31
32
33
34
35
36
37
38
39
40
41
42
43
44
45
46
47
48
49
50
51
52
53
54
55
56
57
58
59
60

1

2
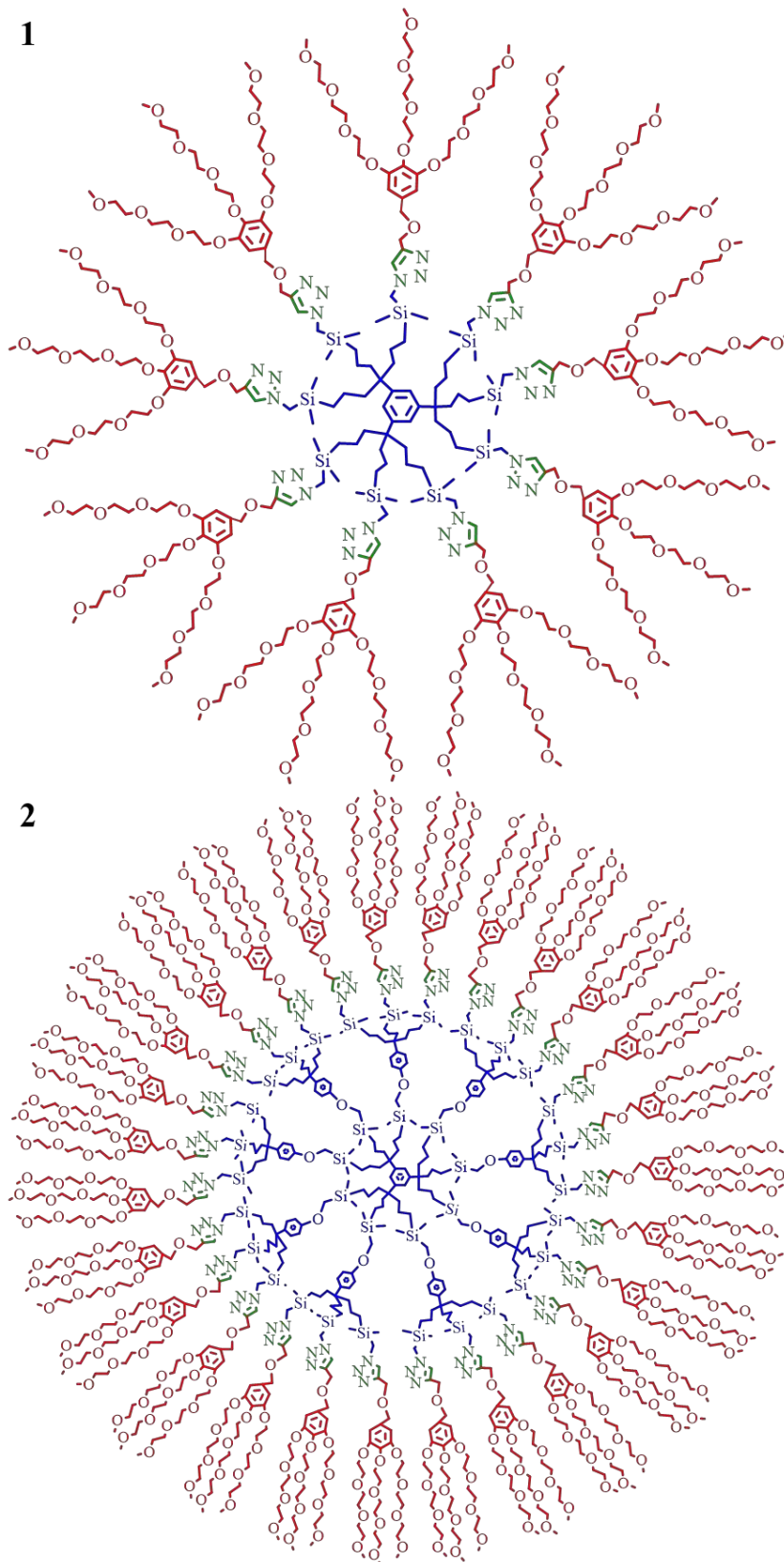
Figure 1. Structures of the dendrimers **1** and **2**.

RESULTS AND DISCUSSION

Synthesis and Characterizations of the Pt-Co/1 NPs.

The synthesis of the "click" dendrimers **1** and **2** was conducted following previous reports.[11] The Pt-Co/**1** NPs were prepared by mixing dendrimer **1** with two precursor metal salts in water followed by stirring 30 min under N_2. Then a freshly prepared aqueous solution of $NaBH_4$ was added, and stirring was continued for 1h (Scheme 1 and SI).

Dendrimer **1**
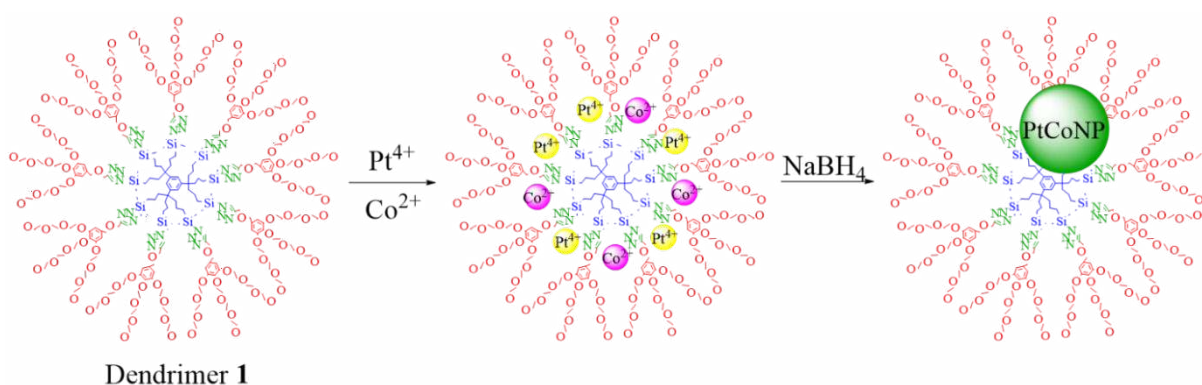
Scheme 1. Synthesis of the Pt-Co/**1** NPs.

TEM images were recorded for the Pt-Co/**1** NPs series, and the average particle sizes were between 1.5 nm and 2.0 nm (Figure S3-5). Very fine and Pt_1Co_1/**1** NPs with narrow size distribution were indicated by TEM with an average size around 2 nm (Figure 2).
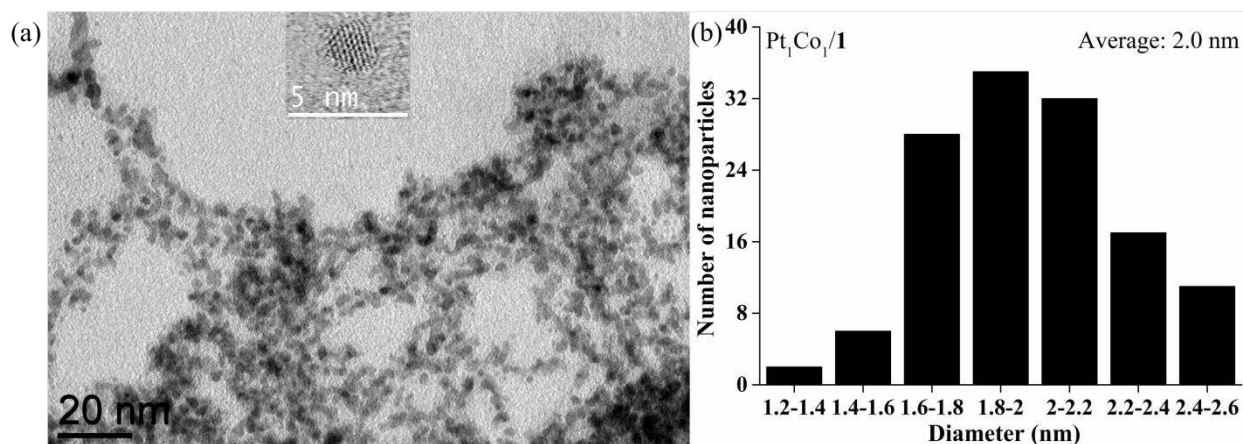
Figure 2. (a) TEM image (insert is the HRTEM image) and (b) size distribution of $Pt_1Co_1/\mathbf{1}$.

A good crystallinity of $Pt_1Co_1/\mathbf{1}$ NPs was confirmed as shown by the clear lattice fringes in HRTEM (Figure 2a insert). The lattice spacing is about 2.2 Å, assuming that the crystallographic plane of the Pt_1Co_1 nanoalloy is {111} (JCPDS 43-1358). The analysis by Energy Dispersive X-Ray Spectroscopy (EDS) of the $Pt_1Co_1/\mathbf{1}$ NPs showed that the Pt and Co elements were present in the 011 area (Figure S6), and the alloy structure of $Pt_1Co_1/\mathbf{1}$ NPs was verified by the HAADF-elemental mapping spectra (Figure S7). The EDS measurements clearly showed that the alloys did not contain any monometallic NPs.

X-ray photoelectron spectroscopy (XPS) analysis of the $Pt_1Co_1/\mathbf{1}$ NPs showed binding energies of 71.1 and 74.4 eV for the $4f_{7/2}$ and $4f_{5/2}$, respectively, indicating the presence of metallic Pt(0) (Figure 3a). In addition a binding energy of 778.6 eV was observed for Co $2p_{3/2}$, showing the existence of Co(0). Another peak around 782.0 eV demonstrated that there is some Co(II) species in the $Pt_1Co_1/\mathbf{1}$ NP sample, probably due to partial oxidation of Co(0) just before or during the XPS experiment (Figure 3b). Indeed, catalysis experiments were conducted just after the syntheses and were not subjected of such sample handling. Therefore it is believed that the Co(II)

species was not present during catalysis. Since the intradendritic triazole ligands are neutral, surface atoms are indeed expected to be Co(0) and Pt(0).
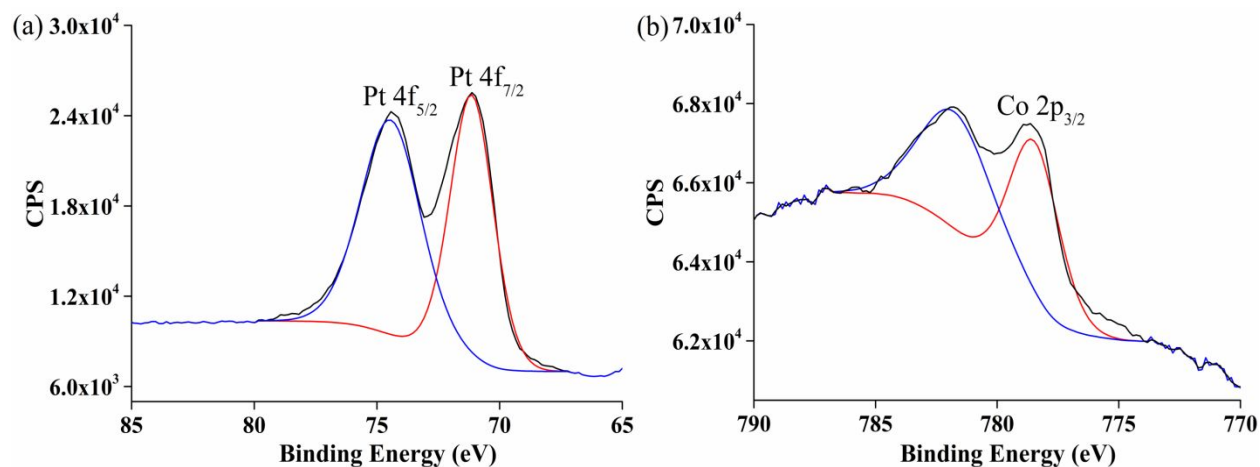
Figure 3. XPS spectrum of (a) Pt 4f and (b) Co 2p in $Pt_1Co_1/1$ nanocatalyst. The presence of some Co(II) most probably results from partial oxidation of the sample just before or during the XPS experiment.

Synergistic catalysis of ammonia borane hydrolysis by various Pt-Co NPs/1.

AB hydrolysis catalyzed by various Pt-Co/**1** NPs (1 mol%) stabilized by dendrimer **1** was conducted at $20 \pm 1°C$ (Table 1, see the kinetics in Figure 4). The compositions of the Pt-Co/**1** NPs were adjusted by varying the molar ratios of the precursors. The naming Pt-Co/**1** NPs will be used in the following text for alloys of NPs containing both PtNPs and CoNPs in any proportions in dendrimer **1**. The proportions of each metal in the alloy will be indicated by the numbers following the Pt and Co symbols (for instance Pt_1Co_1 for equal amounts of Pt and Co in the alloy, etc.).

It is known that Pt is a very efficient metal for the hydrolysis of AB. For example, the PtNPs/**1** led to a TOF value of 120 $mol_{H2} \cdot molcatal^{-1} \cdot min^{-1}$. The performance of CoNPs/**1**, however, was not

very good for this reaction, its TOF value being only 8.8 $mol_{H2}\cdot mol_{catal}^{-1}\cdot min^{-1}$.[7,15] Interestingly,

when Co was introduced to form a Pt-Co alloy NP, the catalyst Pt_1Co_1/**1** led to a TOF value of

163.6 $mol_{H2}\cdot mol_{catal}^{-1}\cdot min^{-1}$ for the hydrolysis of AB. Pt_1Co_1/**1** was the best catalyst among the

whole Pt-Co NP series, and the TOF value decreased from its maximum value when the Co

proportion in the Pt-Co alloy was higher than 1/2. For instance the TOF value of Pt_1Co_2/**1** was 150

$mol_{H2}\cdot mol_{catal}^{-1}\cdot min^{-1}$ for this reaction. All the alloyed Pt-Co NPs gave better results than the

catalyst PtNPs/**1** or CoNPs/**1**. In particuler it is remarkable that the introduction of only 25% of Pt

to Pt-Co alloy led to a better nanocatalyst than PtNPs/**1** alone (Figure 4). In addition, with a

mixture of PtNPs/**1** and CoNPs/**1** (ratio of Pt:Co of 1:1) and a total catalyst amount fixed at 1%,

AB hydrolysis was conducted, and 6 min was needed for complete H_2 generation, which is

slower than 1% Pt_1Co_1/**1** NPs or even than 1% PtNPs/**1** NPs (Figure S14), demonstrating that

there is no synergy with the physical mixture of these CoNPs/**1** and PdNPs/**1**.

Table 1. Core sizes and catalytic efficiencies of various Pt-Co/**1** NPs catalysts in the presence and absence of 0.3 M NaOH at 20 ± 1°C.

Catalyst[a]	Average Size (nm)	TOF[b] ($mol_{H2}\cdot mol_{cat}^{-1}\cdot min^{-1}$)	TOF in the presence of 0.3M NaOH
PtNPs/**1**[c]	2.3	120	78.3
Pt_2Co_1/**1**	1.5	138.5	240
Pt_1Co_1/**1**	2.0	163.6	257.1
Pt_1Co_2/**1**	1.7	150	225
Pt_1Co_3/**1**	1.5	138.5	200
CoNPs/**1**[c]	2.2	8.8	18.8

[a] 1.0 mol % Pt-Co/**1** NPs were used in the catalyzed AB hydrolysis at $20 \pm 1°C$; $NaBH_4$ excess (10/1); [b]

TOF = mol_{H2} released / ($mol_{catalyst} \times$ reaction time$_{(min)}$) related to the all atoms (see also Table S1 for TOF related

to surface atoms); [c] experiment results from a previous study.[7]
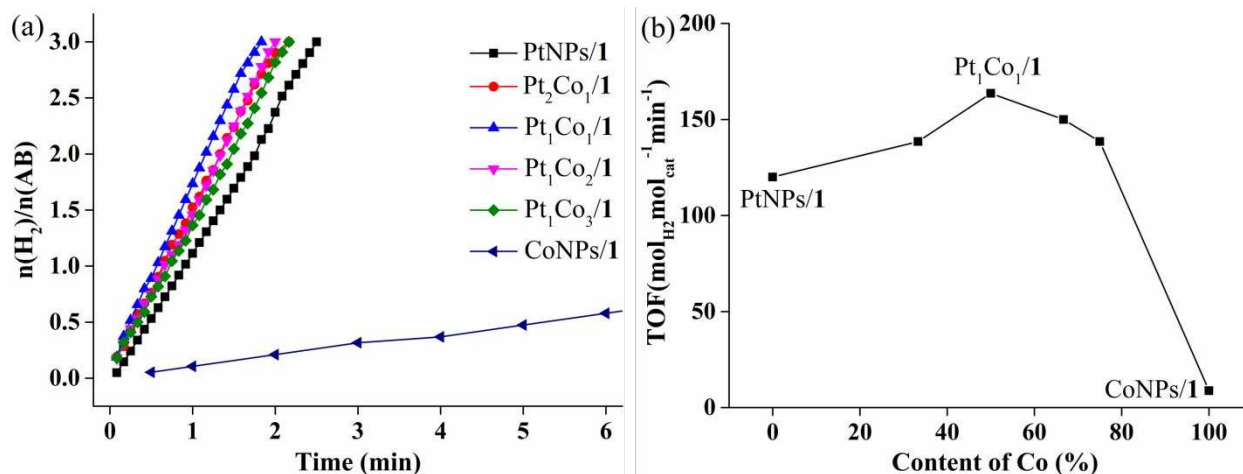
Figure 4. (a) Hydrogen evolution and (b) TOF comparison of NH_3BH_3 by 1 mol% various Pt-Co/**1** nanocatalyst.

The catalytic performances of the monometallic nanocatalysts PtNPs/**1** and CoNPs/**1** toward the

hydrolysis of AB in the presence of NaOH were tested earlier.[7] It was found that NaOH had a

positive influence on the AB hydrolysis catalyzed by CoNPs/**1**, but a negative influence on

PtNPs/**1**. So the hydrolysis of AB catalyzed by Pt-Co/**1** NPs series in the presence of NaOH were

conducted (Figure 5), and the influence of various amounts of NaOH (0.1 M~0.4 M) was further

investigated. The results show that the reaction rates were boosted, higher TOF values being

obtained for Pt-Co/**1** NPs in the presence of NaOH. The best TOF value of 257.1

$mol_{H2} \cdot mol_{catal}^{-1} \cdot min^{-1}$ was reached by Pt_1Co_1/**1** in the presence of 0.3 M NaOH (Table S2 and

Figure S15), and the TOF value decreased with higher NaOH concentration such as 0.4 M.
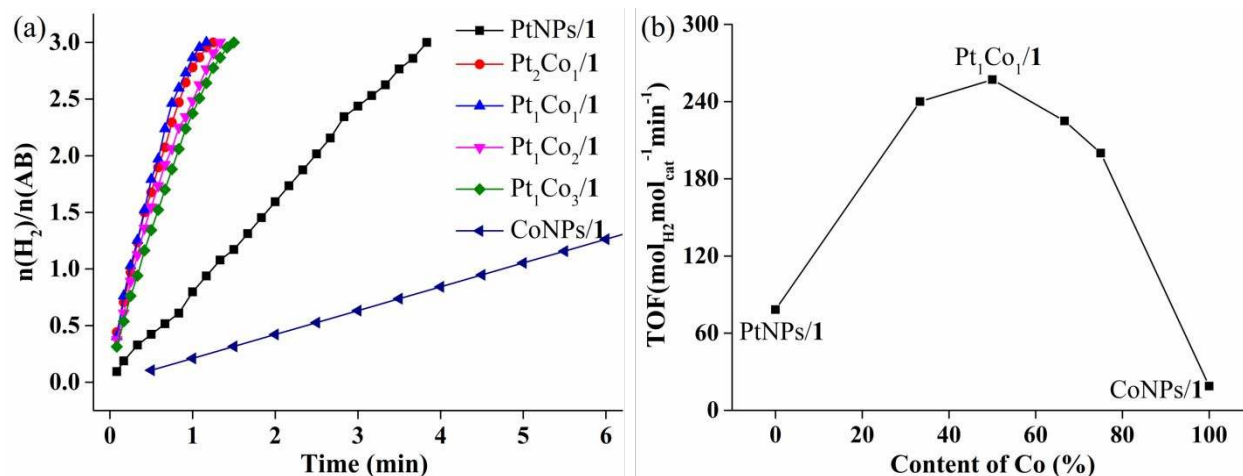
Figure 5. (a) Hydrogen evolution and (b) TOF comparison of NH_3BH_3 by 1 mol% various Pt-Co/**1** nanocatalyst in the presence of 0.3 M NaOH.

The TOF value of PtNPs/**1** decreased from 120 to 78.3 $mol_{H2}·mol_{catal}^{-1}·min^{-1}$ after adding 0.3 M NaOH, but the presence of NaOH had a positive influence on the Pt-Co/**1** NPs series. Remarkably all the Pt-Co/**1** NPs in the various Co/Pt proportions tested present very high synergistic effects between these two metals in the presence of 0.3 M NaOH. The synergy culminates for equal amounts of Co and Pt in the alloy, as in the absence of NaOH, but it is much higher in the presence of NaOH than in its absence in all the proportions of Co/Pt(Figure 6).
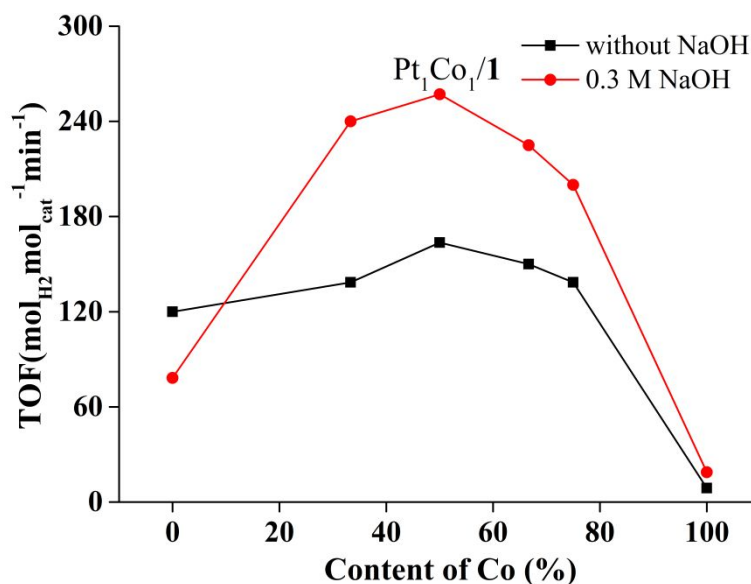
Figure 6. TOF comparison of NH_3BH_3 by 1 mol% various Pt-Co/**1** nanocatalyst in the absence and in the presence of 0.3 M NaOH.

High selectivity of Pt_1Co_1/1 compared to other bi-metallic/1 NPs.

A series of late-transition bimetallic NPs, Rh_1Co_1/**1**, Ru_1Co_1/**1**, Pt_1Ni_1/**1** and Pt_1Cu_1/**1** were synthesized using the same method as that used for the syntheses of the nanocatalysts Pt_1Co_1/**1**. TEM images were recorded for these bimetallic NPs (Figure S8-11). The reactions of AB hydrolysis catalyzed by these bimetallic NPs/**1** (1 mol%) in the absence and presence of 0.3 M NaOH were conducted at $20 \pm 1°C$ (Table 2, see kinetics in Figure 7).

Furthermore, the NPs Pt_1Co_1 stabilized by the first generation dendrimer **2** was synthesized (Figure S12), and the catalytic performances of the Pt_1Co_1 NPs stabilized by two dendrimers were compared for AB hydrolysis. The Pt_1Co_1 NPs stabilized by the zeroth-generation dendrimer **1** showed slightly better results than those obtained using the first-generation dendrimer **2**. The latter led to a TOF value of 100 $mol_{H2} \cdot mol_{catal}^{-1} \cdot min^{-1}$. The dendrimer generation effect[8b] was

found to be weak, probably due to the interdendritic NP stabilization and/or the NP stabilization near the dendrimer periphery.

Table 2. Core sizes and catalytic efficiencies of the bimetallic NPs/**1** catalysts in the presence and absence of 0.3 M NaOH at $20 \pm 1°C$.

Catalyst[a]	Average size (nm)	TOF[b] ($mol_{H2} \cdot mol_{cat}^{-1} \cdot min^{-1}$)	TOF in the presence of 0.3M NaOH
Pt_1Co_1/**1**	2.0	163.6	257.1
Rh_1Co_1/**1**	1.8	94.7	200
Ru_1Co_1/**1**	2.1	33.3	64.3
Pt_1Ni_1/**1**	1.8	94.7	133.3
Pt_1Cu_1/**1**	1.8	12	17.6
Pt_1Co_1/**2**	2.0	100	163.6

[a] 1.0 mol % bimetallic NPs were used in the catalyzed AB hydrolysis at $20 \pm 1°C$; $NaBH_4$ excess (10/1); [b] TOF = mol_{H2} released / ($mol_{catalyst} \times$ reaction time$_{(min)}$) related to all atoms (see also Table S3 for TOF related to surface atoms).

The comparison showed that Pt_1Co_1/**1** exhibited the best efficiency among these bimetallic NP catalysts, followed by the nanocatalysts Rh_1Co_1/**1** and Pt_1Ni_1/**1**. The same TOF value of 94.7 $mol_{H2} \cdot mol_{catal}^{-1} \cdot min^{-1}$ was achieved by the latter two catalysts. The TOF value of PtNPs/**1** was 120 $mol_{H2} \cdot mol_{catal}^{-1} \cdot min^{-1}$, which indicated that there was no synergy between Pt and Ni. A similar conclusion was reached for Rh and Co, because the TOF value of RhNPs/1 was 120 $mol_{H2} \cdot mol_{catal}^{-1} \cdot min^{-1}$.[7] All the AB hydrolysis reactions catalyzed by these bimetallic NPs were accelerated in the presence of 0.3 M NaOH, as shown by comparison with the results obtained in the absence of NaOH (Figure S16-17).
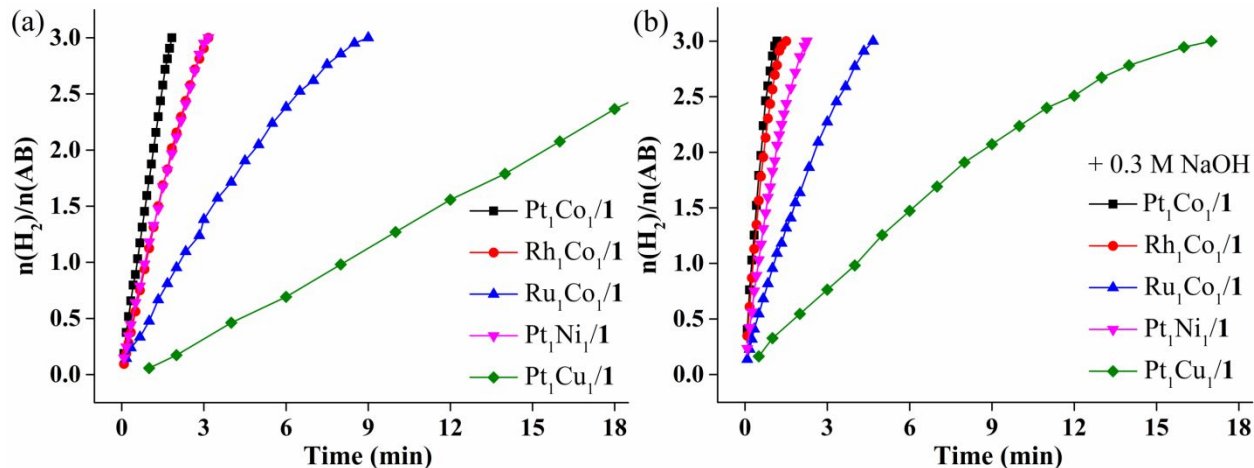
Figure 7. Comparison of the hydrogen evolution upon reaction between NH_3BH_3 and H_2O catalyzed by 1 mol% bimetallic NPs/**1** (a) in the absence of NaOH and (b) in the presence of 0.3 M NaOH.

The durability of the best catalyst Pt_1Co_1/**1** has been checked because of its importance for practical applications (Figure 8). Another equivalent of AB (1 mmol) was injected into the flask after the end of a reaction, and the second round was started. The AB hydrolysis reactions were repeated several times in this way. The results showed that after five cycles the Pt_1Co_1/**1** nanocatalyst still presented a good catalytic property for AB hydrolysis. After the 5th catalyst recycling the size of the catalyst has now been re-measured by TEM indicating size increase (Figure S13). It is believed that NP size increase and agglomeration and concomitant activity decrease in the 5th recycling shown in Figure 8 are due to the accumulation of the sodium and ammonium products of the reaction adsorbing on the NP surface.
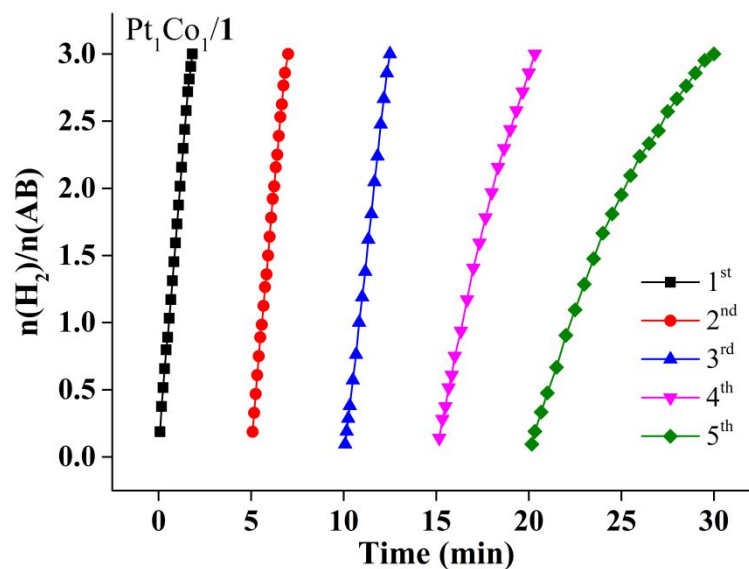
Figure 8. Plots of volume of H_2 vs. time for the hydrolysis of AB catalyzed by 1 mol% $Pt_1Co_1/\mathbf{1}$ during the reusability tests.

Mechanistic studies for the AB hydrolysis reaction catalyzed by $Pt_1Co_1/\mathbf{1}$

The determination of the second Damköhler number ($Da_{II} = 0.02$), much lower than unity, allowed ruling out mass-transfer-induced diffusion control (see S.I.). The slope of the logarithmic plot of H_2 generation vs. concentration of $Pt_1Co_1/\mathbf{1}$ is 1.16 (Figure 9), showing that the reaction is first order in catalyst concentration.
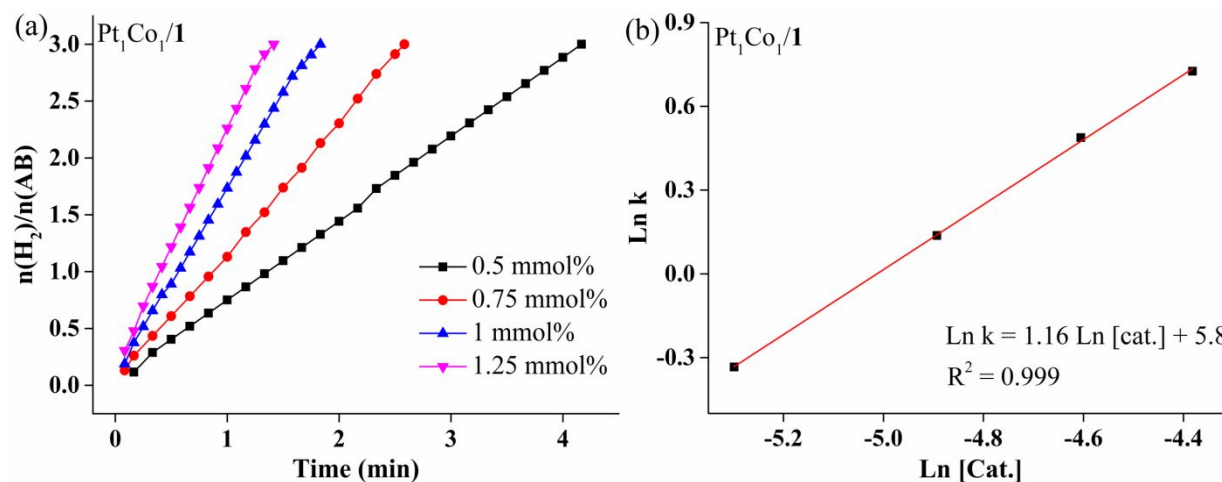
Figure 9. Time plots of the catalytic dehydrogenation of AB by $Pt_1Co_1/\mathbf{1}$ nanocatalyst with various catalysts (a), and plot of hydrogen generation rate vs. concentration of the nanocatalyst $Pt_1Co_1/\mathbf{1}$ both in natural logarithmic scale (b).

The reaction is zero order in AB concentration (the slope of the logarithmic plot of H_2 generation vs. concentration of AB is a nearly horizontal line; slope: 0.09 in Figure 10), which rules out activation of AB alone in the rate-determining step.
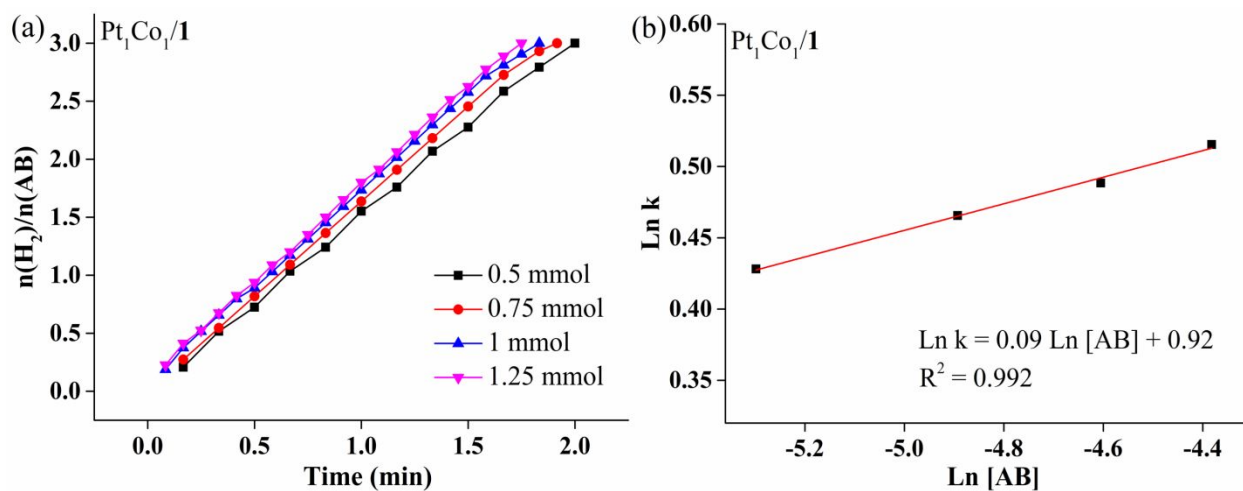
Figure 10. Plots of volume of H_2 generated vs. time for AB hydrolysis catalyzed by 1 mol% of $Pt_1Co_1/\mathbf{1}$ nanocatalyst (a), and plot of the hydrogen generation rate vs. the concentration of AB both in natural logarithmic scale (b).

The measure of the time dependence of H_2 generation at various temperatures led to the determination of a low activation energy (E_a) of 28.8 kJ·mol^{-1} for Pt_1Co_1/**1** (Figure 11 and see calculation in the SI).
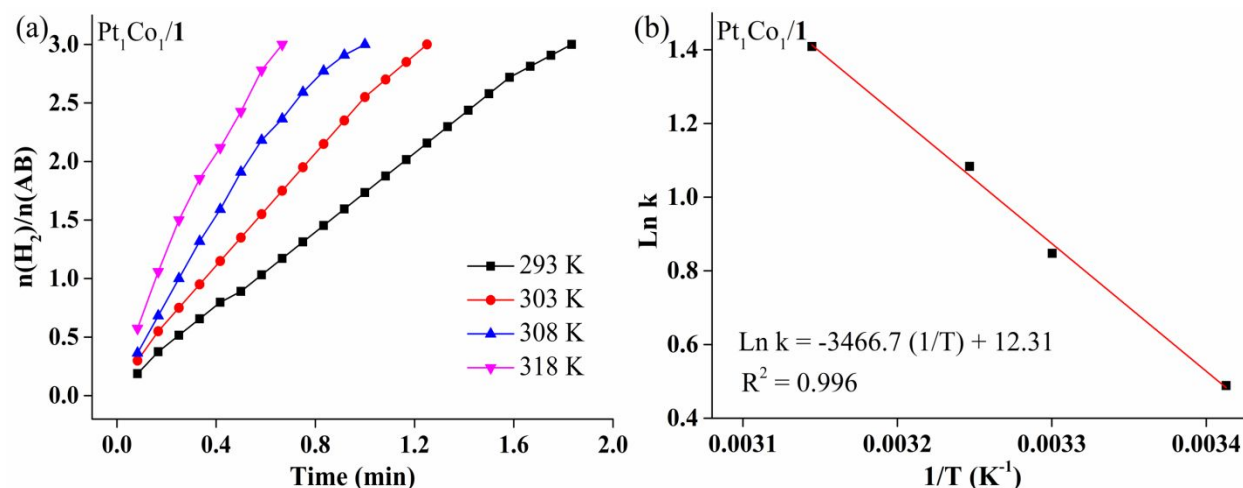
Figure 11. Plots of the volume of H_2 vs. time for the hydrolysis of AB at various temperatures catalyzed by 1 mol% of Pt_1Co_1/**1** catalyst (a), and Arrhenius plots obtained from the kinetic data (b).

The isotopic experiment using D_2O instead of H_2O was conducted for the Pt_1Co_1/**1**-catalyzed AB hydrolysis, and the kinetic results are presented in Figure 12, showing a large kinetic isotope effect (KIE) of 2.46. The kinetic studies, and in particular the latter experiment, suggests cleavage of a water O-H bond in the rate-determining step.
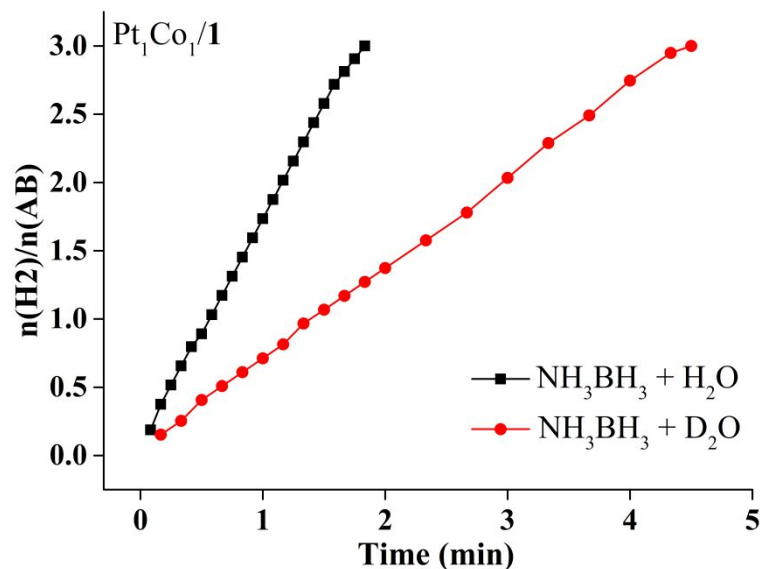
Figure 12. Hydrogen evolution from NH_3BH_3 with H_2O and D_2O catalyzed by 1 mol% of the nanocatalyst Pt_1Co_1/**1** (KIE = 2.46).

In conclusion the results obtained here show a strong and remarkable bimetallic synergy between cobalt and platinum optimized in the Co_1Pt_1 alloy, in particular in the presence of 0.3 M NaOH. This synergy also involves the "click" dendrimer supports, in particular the intradendritic 1,2,3-triazole ligands that have proven to be essential.[9g, 11c, 16] Previously the coordination of various transition-metal NPs to the triazole ligands of the same dendrimer **1** near the dendrimer periphery has been shown to be highly beneficital for NP catalysis. This has been demonstrated in very efficient catalysis by PdNP/**1** with ppm Pd amounts for various carbon-carbon cross coupling reactions (Miyaura-Suzuki, Sonogashira, and Heck),[11c, 16b-d] by CuNP/**1** for "click" reactions,[9g, 16e] and by a variety of transition metal NPs/**1** for nitrophenol reduction.[16f-g] Altogether these "click" dendrimer **1** and **2**, i.e. containing the intradendritic 1,2,3-triazole ligands, have been shown to boost catalysis of a various reactions by molecular, ionic and NP catalysts. The electronic donicity of the triazole ligand onto the NP surfaces is responsible for the superior catalytic activity of these

NP surfaces,[16e] in particular here for the difficult oxidative addition of the water O-H bond in the rate-determining step. Note that the fully stable "click" dendrimers **1** and **2** are also used in catalytic amounts and recovered unchanged in the aqueous phase at the end of the reactions. The present results are among the very best obtained compared to results on related bimetallic nanocatalysts in the literature as shown in the comparison Table S4.

The practical usages of hydrogen produced in the AB hydrolysis reaction are not only for hydrogen storage, but also for its direct use *in situ*, for tandem reactions, and for mechanistic studies of the AB hydrolysis reaction. Examples of the latter applications are shown here. Tandem reactions were conducted for the hydrogenation of styrene with hydrogen generated from AB hydrolysis with D_2O. In a sealed two-chamber system (Figure S18), the hydrogen was produced from AB with D_2O, the reaction being catalyzed by Pt_1Co_1/**1** in the left tube. This hydrogen is used for the hydrogenation[17] of styrene catalyzed by Ni_2Pt@ZIF-8[18] in the right tube (Figure 13, see details in the Supporting Information). The reaction mixture of styrene hydrogenation was stirred at 50 °C for 12 h, then the ^{1}H NMR and GC mass spectra of the hydrogenation product were checked. The integration of the ^{1}H NMR peak around 1.2 and 2.6 ppm showed a reduced intensity compared to that of ethylbenzene in its ^{1}H NMR spectrum (Figure S19). Three peaks around 106, 107 and 108 were found the in mass spectrum (Figure S20), showing that there were three hydrogenation products of styrene, which contained respectively 0, 1 and 2 D atoms in the ethyl substituent, respectively.
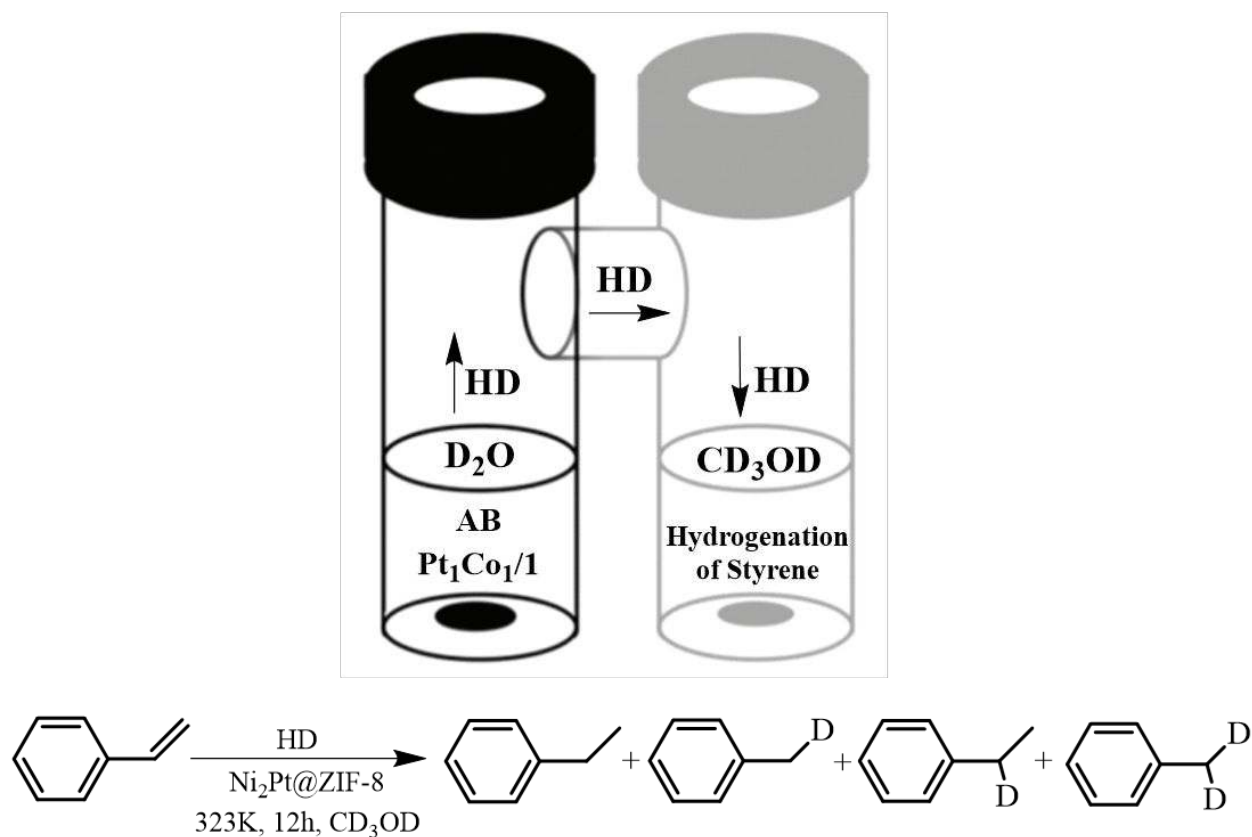
Figure 13. Tandem reaction for hydrogenation with "HD" generated from AB catalyzed by Pt$_1$Co$_1$/**1**. On the arrow, "HD" represents a mixture of H$_2$, HD and D$_2$ (see text).

Several mechanisms have been proposed for the late transition-metal NP-catalyzed hydrolysis of AB. Xu et al proposed attack of H$_2$O onto an activated complex provoking B-N cleavage, followed by hydrolysis of NH$_3$ generating H$_2$.[3] Jagirdar's group proposed attack of H$_2$O on a transient M-H bond by analogy with the hydrolysis of BH$_4^-$.[19] Na and Ma also proposed a similar mechanism related to BH$_4^-$ hydrolysis.[20] Fu suggested the formation of BH$_3$OH$^-$NH$_4^+$ followed by H$_2$O attack to generate H$_2$.[21] Chen[2] and Fu[18] proposed cleavage of the O-H bond of water in the rate-determining step.

A mechanistic proposal based on our experiment results follows. An essential mechanistic feature appears to be the hydrogen bonding between AB and water, i.e. $[H_3NBH_2H]\ldots H\text{-}OH$. Such H-bonding results from the hydridic property of the B-H bond. A hydridic BH is proposed to transfer its H atom to the NP surface, which formally corresponds to an oxidative addition of this B-H bond onto the surface. Oxidative addition of the water O-H bond occurs in the rate-determining step, as essentially indicated from the large KIE (k_H/k_D = 2.46) with D_2O. The favorable OH^- effect for bimetallic NPs/**1** is consistent with coordination of OH^- onto the NP surface, which makes the NP more electron-rich and beneficial to the oxidative addition of H_2O. On the contrary, OH^- has a negative effect on AB hydrolysis catalyzed by PtNPs/**1**. The reason probably is that the hydrogen bonding between AB and H_2O is sufficient to favor O-H oxidative addition by the most electron-rich PtNPs surface. Accordingly there is no need at this point to further enrich the electron density of the monometallic PtNP surface by OH^- coordination. Furthermore, the added OH^- would partly occupy the surface active sites of PtNPs, inhibiting the oxidative addition of the water O-H bond, thereby decelerating the reaction. In this step, synergy between a Pt atom and a Co is likely to operate. The more electron-rich Pt NP atom would most probably form both Pt-H bonds due to the high strength of the Pt-H bonds, while the less electron-rich Co atom would bind the electron-rich OH group to form a Co-OH bond. The di-hydride-nanoparticle species would then easily form H_2 by reductive elimination as is well known in transition-metal organometallic chemistry and catalysis.[22] The tandem reaction with D_2O showing deuteration of the ethylbenzene products confirms H/D exchange subsequently to O-D cleavage and H/D scrambling on the nanoparticle surface before reductive elimination. Given the KIE value and the favorable effect of OH^- on the reaction rate, it is not possible that protonation of AB by water (heterolytic H_2O or D_2O cleavage) occurs before the rate-limiting step. A tentative reaction mechanism is represented

in Scheme 2. Reductive elimination of H_2 is accompanied by reductive elimination of the two fragments NH_3BH_2- and OH- to form the hydroxy intermediate NH_3BH_2OH. This first overall step (a) thus corresponds to the substitution in ammonia borane of an H atom by OH on boron. Each of the two subsequent H_2 evolution steps (b) and (c) are proposed to proceed by the same mechanism leading to adsorbed $B(OH)_3NH_3$ that upon hydrolysis produces $NH_4^+B(OH)_4^-$ (d).
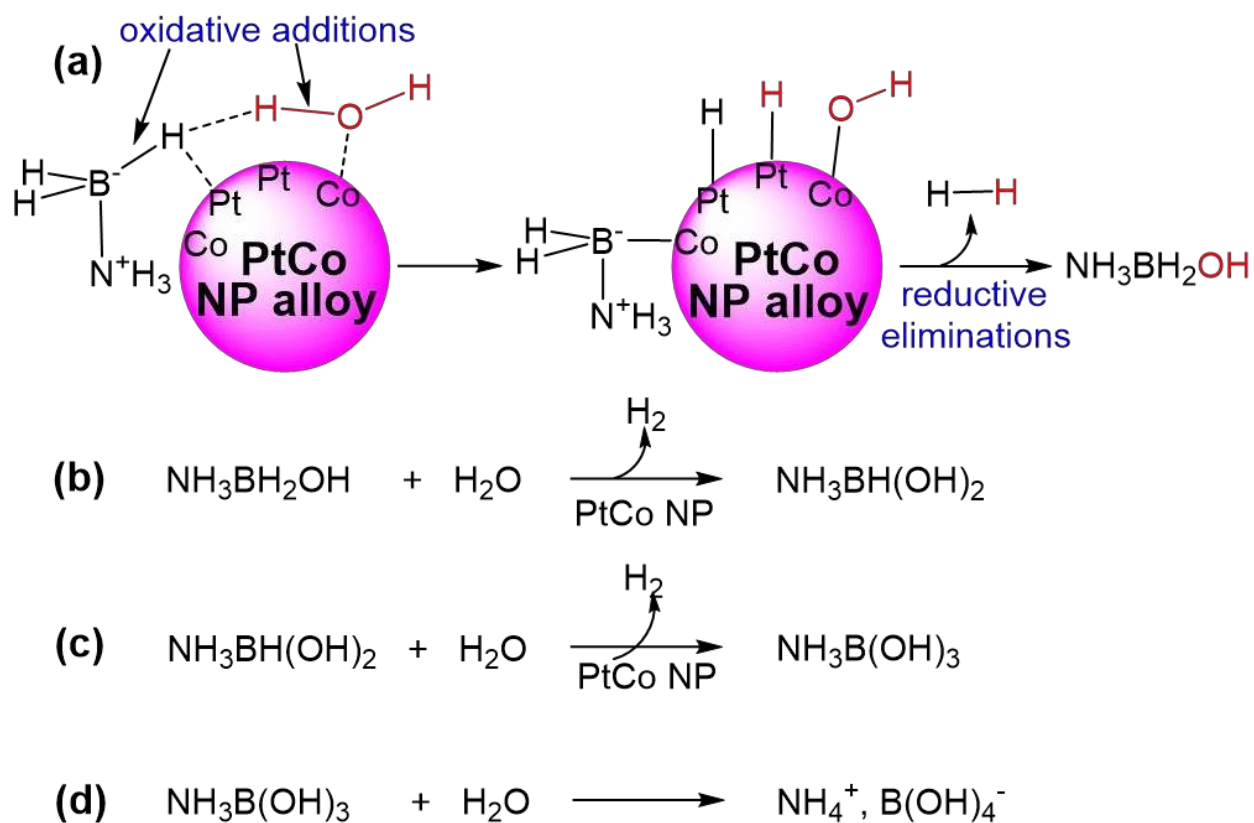
Scheme 2. Proposed mechanism for the hydrolysis of AB catalyzed by $Pt_1Co_1/\mathbf{1}$.

CONCLUDING REMARKS

In conclusion, two generations of "click" dendrimers stabilized various bimetallic NPs that catalyze AB hydrolysis producing 3 mol hydrogen. The reaction is zero order in AB and first order in NP catalyst. A remarkably highly positive synergistic effect is discovered for the nanocatalysts Pt-Co/**1** containing various proportions of Co and Pt NPs in the nanoalloys, so that the presence of even down to 25% Pt in the nanocatalyst Pt-Co/**1** produces a catalyst that is more efficient than PtNP/**1**. NaOH increases the reaction rate, except for PtNPs. The maximum synergistic effect is disclosed both in the absence and presence of 0.3 M NaOH with nanoalloys containing equal amounts of Co and Pt. This dramatic synergy between Pt and Co is highly selective compared to other bimetallic NPs stabilized by the dendrimer **1**. With other supports these PtCo nanoalloys are on the contrary less efficient. Thus the synergy also involves the dendrimer, in particular its intradendritic 1,2,3-triazole ligands that activate the NP surface. The TOF value reached with Pt_1Co_1/**1** is 476.2 $mol_{H2} \cdot mol_{catal.}^{-1} \cdot min^{-1}$ (952.4 $mol_{H2} \cdot mol_{Pt}^{-1} \cdot min^{-1}$) for the production of 3 mol H_2 completed in 70 s at 20°C (Table S1), one of the best results ever recorded. The large kinetic isotope effect ($k_H/k_D = 2.46$) with D_2O indicates that the cleavage of the O-H bond of water occurs in the rate-determining step. This mechanism is suggested to involve oxidative addition of a hydridic B-H bond of AB to the NP facilitated by hydrogen bonding between a B-H bond of AB and a H atom of water. This is followed by reductive elimination of H_2 and NH_3BH_2OH and two analogous overall steps before hydrolysis to $NH_4^+B(OH)_4^-$. The tandem reaction with D_2O that involves AB hydrolysis-styrene hydrogenation producing deuterated ethylbenzenes confirms O-D cleavage in the rate-limiting step followed by H/D scrambling on the nanoparticle surface before reductive elimination of HD, H_2, and D_2.

ASSOCIATED CONTENT

Supporting Information

The Supporting Information is available free of charge on the ACS Publications website at DOI:

XXX. General data, experimental details, characterizations and kinetics of AB hydrolysis.

AUTHOR INFORMATION

Corresponding Author

didier.astruc@u-bordeaux.fr

Notes

The authors declare no competing financial interest.

REFERENCES

(1) (a) Staubitz, A.; Robertson, A. P. M.; Manners, I. Ammonia-Borane and Related

Compounds as Dihydrogen Sources, *Chem. Rev.* **2010**, *110*, 2793-4124. (b) Rossin, A.; Perruzini,

M. Ammonia-Borane and Amine-Borane Dehydrogenation Mediated by Complex Metal

Hydrides. *Chem. Rev.* **2016**, *116*, 8848-8872.

(2) Chen, W.; Li, D.; Wang, Z.; Qian, G.; Sui, Z.; Duan, X.; Zhou, X.; Yeboah, I.; Chen, D. Reaction mechanism and kinetics for hydrolytic dehydrogenation of ammonia borane on a Pt/CNT catalyst. *AIChE J.* **2017**, *63*, 60-65.

(3) For a seminal report see: Xu, Q.; Chandra, M. Catalytic activities of non-noble metals for hydrogen generation from aqueous ammonia-borane at room temperature. *J. Power Sources.* **2006**, *163*, 364-370.

(4) Reviews: (a) Hamilton, C. W.; Baker, R. T.; Staubitz, A.; Manners, I. B-N compounds for chemical hydrogen storage. *Chem. Soc. Rev.* **2009**, *38*, 279-293. (b) Zhu, Q.-L.; Xu, Q. Liquid organic and inorganic chemical hydrides for high-capacity hydrogen storage. *En. Environ. Sci.* **2015**, *8*, 478-512. (c) Zhan, W.-W.; Zhu, Q.-L.; Xu, Q. Dehydrogenation of Ammonia Borane by Metal Nanoparticle Catalysts. *ACS Catal.* **2016**, *6*, 6892-6905. (d) Akbayrak, S.; Özkar, S. Ammonia borane as hydrogen storage materials. *Int. J. Hydrog. En.* **2018**, *43*, 18592-18606.

(5) (a) Lee, J.; Farha, O. K.; Roberts, J.; Scheidt, K. A.; Nguyen, S. T.; Hupp, J. T. Metal-organic framework materials as catalysts. *Chem. Soc. Rev.* **2009**, *38*, 1450-1459. (b) Farrusseng, D.; Aguado, S.; Pinel, C. Metal-organic frameworks: opportunities for catalysis. *Angew. Chem., Int. Ed.* **2009**, *48*, 7502-7513. (c) Rakap, M.; Ozkar, S. Hydrogen generation from the hydrolysis of ammonia-borane using intrazeolite cobalt(0) nanoclusters catalyst. *Int. J. Hydrog. Energy* **2010**, *35*, 3341-3346. (d) Dhakshinamoorthy, A.; Garcia, H. Catalysis by metal nanoparticles embedded on metal-organic frameworks. *Chem. Soc. Rev.* **2012**, *41*, 5262-5284. (e) Liu, J.; Chen, L.; Cui, H.; Zhang, J.; Zhang, L.; Su, C. Y. Applications of metal-organic frameworks in heterogeneous supramolecular catalysis. *Chem. Soc. Rev.* **2014**, *43*, 6011-6061. (f) Chughtai, A. H.; Ahmad, N.; Younus, H. A.; Laypkov, A.; Verpoort, F. Metal-organic frameworks: versatile heterogeneous catalysts for efficient catalytic organic transformations. *Chem. Soc. Rev.* **2015**, *44*, 6804-6849. (g)

Zeng, L.; Guo, X.; He, C.; Duan, C. Metal-Organic Frameworks: Versatile Materials for Heterogeneous Photocatalysis. *ACS Catal*. **2016**, *6*, 7935-7947.

(6) (a) Xu, Q.; Chandra, M. A. portable hydrogen generation system: Catalytic hydrolysis of ammonia-borane. *J. Alloy. Compd*. **2007**, *446*, 729-732. (b) Aijaz, A.; Karkamkar, A.; Choi, Y. J.; Tsumori, N.; Rönnebro, E.; Autrey, T.; Shioyama, H.; Xu, Q. Immobilizing highly catalytically active Pt nanoparticles inside the pores of metal-organic framework: a double solvents approach. *J. Am. Chem. Soc*. **2012**, *134*, 13926-13929. (c) Khalily, M. A.; Eren, H.; Akbayrak, S.; Susapto, H. H.; Biyikli, N.; Özkar, S.; Guler, M. O. Facile Synthesis of Three-Dimensional Pt-TiO_2 Nano-networks: A Highly Active Catalyst for the Hydrolytic Dehydrogenation of Ammonia-Borane. *Angew. Chem. Int. Ed.* **2016**, *55*, 12257-12261. (d) Chen, W.; Li, D.; Peng, C.; Qian, G.; Duan, X.; Chen, D.; Zhou, X. Mechanistic and kinetic insights into the Pt-Ru synergy during hydrogen generation from ammonia borane over PtRu/CNT nanocatalysts. *J. Catal.* **2017**, *356*, 186-196. (e) Wang, X.; Liu, D.; Song, S.; Zhang, H. Synthesis of highly active Pt-CeO_2 hybrids with tunable secondary nanostructures for the catalytic hydrolysis of ammonia borane. *Chem. Commun.* **2012**, *48*, 10207-10209. (f) Wang, C.; Tuminetti, J.; Wang, Z.; Zhang, C.; Ciganda, R.; Moya, S.; Ruiz, J.; Astruc, D. Hydrolysis of Ammonia-Borane over Ni/ZIF-8 Nanocatalyst: High Efficiency, Mechanism, and Controlled Hydrogen Release. *J. Am. Chem. Soc.* **2017**, *139*, 11610-11615.

(7) Wang, Q.; Fu, F.; Escobar, A.; Moya, S.; Ruiz, J.; Astruc, D. "Click" Dendrimer-Stabilized Nanocatalysts for Efficient Hydrogen Release upon Ammonia-Borane Hydrolysis. *ChemCatChem*. **2018**, *10*, 2673-2680.

(8) (a) Oosterom, G. E.; Reek, J. N.; Kamer, P. C.; van Leeuwen, P. W. Transition Metal Catalysis Using Functionalized Dendrimers. *Angew. Chem., Int. Ed.* **2001**, *40*, 1828-1849. (b) Astruc, D.; Boisselier, E.; Ornelas, C. Dendrimers Designed for Functions: From Physical,

Photophysical and Supramolecular Properties to Applications in Sensing, Catalysis, Molecular Electronics, Photonics and Nanomedicine. *Chem. Rev.* **2010**, *110*, 1857-1959. (c) Wang, D.; Astruc, D. Dendritic catalysis-Basic concepts and recent trends. *Coord. Chem. Rev.* **2013**, *257*, 2317-2334.

(9) (a) Crooks, R. M.; Zhao, M.; Sun, L.; Chechik, V.; Yeung, L. K. Dendrimer-encapsulated metal nanoparticles: synthesis, characterization, and applications to catalysis. *Acc. Chem. Res.* **2001**, *34*, 181-190. (b) Astruc, D; Lu, F.; Ruiz, J. Nanoparticles as recyclable catalysts: the frontier between homogeneous and heterogeneous catalysis. *Angew. Chem., Int. Ed.* **2005**, *44*, 7852-7872. (c) Astruc, D. Palladium Catalysis Using Dendrimers: Molecular Catalysts vs. Nanoparticles. *Tetrahedron Asym.* **2010**, *21*, 1041-1054. (d) Myers, V. S.; Weir, M. G.; Carino, E. V.; Yancey, D. F.; Pande, S.; Crooks, R. M. Dendrimer-encapsulated nanoparticles: new synthesis and characterization methods and catalytic applications. *Chem. Sci.* **2011**, *2*, 1632-1646. (e) Wang, D.; Li, Y. Bimetallic Nanocrystals: Liquid-phase Synthesis and Catalytic Applications. *Adv. Mater.* **2011**, *23*, 1044-1060. (f) Zaera, F. Nanostructured materials for applications in heterogeneous catalysis. *Chem. Soc. Rev.* **2013**, *42*, 2746-2762. (g) Deraedt, C.; Pinaud, N.; Astruc, D. Recyclable Catalytic Dendrimer Nanoreactor for Part-Per-Million Cu(I) Catalysis of "click" Reactions in Water. *J. Am. Chem. Soc.* **2014**, *136*, 12092-12098. (h) Deraedt, C.; Ye, R.; Ralston, W. T.; Toste, F. D.; Somorjai, G. A. Dendrimer-Stabilized Metal Nanoparticles as Efficient Catalysts for Reversible Dehydrogenation/Hydrogenation of Heterocycles. *J. Am. Chem. Soc.* **2018**, *139*, 18084-18092. (i) Shiffrina, Z. B.; Bronstein, L. M. Magnetically Recoverable Catalysts: Beyond Magnetic Separation. *Frontiers Chem.* **2018**, *6*, 298.

(10) Aranishi, K.; Zhu, Q.-L.; Xu, Q. Dendrimer-Encapsulated Cobalt Nanoparticles as High-Performance Catalysts for the Hydrolysis of Ammonia Borane. *ChemCatChem.* **2014**, *6*, 1375-1379.

(11) (a) Diallo, A. K.; Boisselier, E.; Liang, L.; Ruiz, J.; Astruc, D. Dendrimer-induced Molecular Catalysis in Water: the Example of Olefin Metathesis. *Chem. Eur. J.* **2010**, *16*, 11832-11835. (b) Boisselier, E.; Diallo, A. K.; Salmon, L.; Ornelas, C.; Ruiz, J.; Astruc, D. Encapsulation and Stabilization of Gold Nanoparticles with "Click" Polyethyleneglycol Dendrimers. *J. Am. Chem. Soc.* **2010**, *132*, 2729-2742. (c) Deraedt, C.; Salmon, L.; Etienne, L.; Ruiz J.; Astruc, D. "click" dendrimers as efficient nanoreactors in aqueous solvent: Pd nanoparticle stabilization for sub-ppm Pd catalysis of Suzuki-Miyaura reactions of aryl bromides. *Chem. Commun.* **2013**, *49*, 8169-8171.

(12) (a) Yan, J. M.; Zhang, X.-B.; Akita, T.; Haruta, M.; Xu, Q. One-Step Seeding Growth of Magnetically Recyclable Au@Co Core-Shell Nanoparticles: Highly Efficient Catalyst for Hydrolytic Dehydrogenation of Ammonia Borane. *J. Am. Chem. Soc.* **2010**, *132*, 5326-5327. (b) Ge, Y.; Ye, W.; Shah, Z. H.; Lin, X.; Lu, R.; Zhang, S. PtNi/NiO Clusters Coated by Hollow Sillica: Novel Design for Highly Efficient Hydrogen Production from Ammonia-Borane. *ACS Appl. Mater. Interfaces* **2017**, *9*, 3749-3756. (c) Fan, G.; Li, X.; Ma, Y.; Zhang, Y.; Wu, J.; Xu, B.; Sun, T.; Gao, D.; Bi, J. Magnetic, recyclable $Pt_yCo_{1-y}/Ti_3C_2X_2$ (X = O, F) catalyst: a facile synthesis and enhanced catalytic activity for hydrogen generation from the hydrolysis of ammonia borane. *New J. Chem.* **2017**, *41*, 2793-2799. (d) Cui, X.; Li, H.; Yu, G.; Yuan, M.; Yang, J.; Xu, D.; Hou, Y.; Dong, Z. Pt coated Co nanoparticles supported on N-doped mesoporous carbon as highly efficient, magnetically recyclable and reusable catalyst for hydrogen generation from ammonia borane. *Int. J. Hydrog. Energy* **2017**, *42*, 27055-27065. (e) Karaca, T.; Sevim, M.; Metin,

Ö. Facile Synthesis of Monodisperse Copper-Platinum Alloy Nanoparticles and Their Superb Catalysis in the Hydrolytic Dehydrogenation of Ammonia Borane and Hydrazine Borane. *ChemCatChem.* **2017**, *9*, 4185-4190. (f) Zhan, W.-W.; Zhu, Q.-L.; Dang, S.; Liu, Z.; Kitta, M.; Suenaga, K.; Zheng, L.-S.; Xu, Q. Synthesis of Highly Active Sub-Nanometer Pt@Rh Core-Shell Nanocatalyst via a Photochemical Route: Porous Titania Nanoplates as a Superior Photoactive Support. *Small* **2017**, *13*, 1603879. (g) Ke, D.; Wang, J.; Zhang, H.; Li, Y.; Zhang, L.; Zhao, X.; Han, S. Fabrication of Pt-Co NPs supported on nanoporous graphene as high-efficient catalyst for hydrolytic dehydrogenation of ammonia borane. *Int. J. Hydrog. Energy* **2017**, *42*, 26617-26625.

(13) Fu, Z.-C.; Xu, Y.; Chan, S. L.-F.; Wang, W.-W.; Li, F.; Liang, F.; Chen, Y.; Lin, Z.-S.; Fu, W.-F. Che, C.-M. Highly efficient hydrolysis of ammonia borane by anion ($^-$OH, F$^-$, Cl$^-$)-tuned interactions between reactant molecules and CoP nanoparticles. *Chem. Commun.* **2017**, *53*, 705-708.

(14) (a) Keaton, R. J.; Blacquiere, J. M.; Baker, R. T. Base Metal Catalyzed Dehydrogenation of Ammonia-Borane for Chemical Hydrogen Storage. *J. Am. Chem. Soc.* **2007**, *129*, 1844-1845. (b) Bhattacharya, P.; Krause, J. A.; Guan, H. Mechanistic Studies of Ammonia Borane Dehydrogenation Catalyzed by Iron Pincer Complexes. *J. Am. Chem. Soc.* **2014**, *136*, 11153-11161. (c) Buss, J. A.; Edouard, G. A.; Cheng, C.; Shi, J.; Agapic, T. Molybdenum Catalyzed Ammonia Borane Dehydrogenation: Oxidation State Specific Mechanisms. *J. Am. Chem. Soc.* **2014**, *136*, 11272-11275.

(15) For good CoNPs catalysts in AB hydrolysis, see the reviews in ref 3 and (a) Umegaki, T.; Yan, J. M.; Zhang, X. B.; Shioyama, H.; Kuriyama, N.; Xu, Q. Co-SiO$_2$ nanosphere-catalyzed hydrolytic dehydrogenation of ammonia borane for chemical hydrogen storage. *J. Power Sources* **2010**, *195*, 8209-8214. (b) Yan, J. M.; Zhang, X. B.; Shioyama, H.; Xu, Q. Room temperature

hydrolytic dehydrogenation of ammonia borane catalyzed by Co nanoparticles. *J. Power Sources* **2010**, *195*, 1091-194. (c) Rakap, M., Özkar S. Hydroxyapatite-supported cobalt(0) nanoclusters as efficient and cost-effective catalyst for hydrogen generation from the hydrolysis of both sodium borohydride and ammonia-borane. *Catal. Today* **2012**, *183*, 17-25. (d) Zahmakiran, M.; Özkar, S. Transition Metal Nanoparticles in Catalysis for the Hydrogen Generation from the Hydrolysis of Ammonia-Borane. *Top. Catal*. **2013**, *56*, 1171-1183. (e) Hu, J. T.; Chen, Z. X.; Li, M. X.; Zhou, X. H.; Lu, H. B. Amine-Capped Co Nanoparticles for Highly Efficient Dehydrogenation of Ammonia Borane. *ACS Appl. Mater. Interfaces* **2014**, *6*, 13191-13200. (f) Yang, L.; Cao, N.; Du, C.; Dai, H. M.; Hu, K.; Luo, W.; Cheng, G. Z. Graphene supported cobalt(0) nanoparticles for hydrolysis of ammonia borane. *Mater. Lett*. **2014**, *115*, 113-116. (g) Wang, H. X.; Zhao, Y. R.; Cheng, F. Y.; Tao, Z. L.; Chen, J. Cobalt nanoparticles embedded in porous N-doped carbon as long-life catalysts for hydrolysis of ammonia borane. *Catal. Sci. Technol*. **2016**, *6*, 3443-3448. (h) Zhou, L. M.; Meng, J.; Li, P.; Tao, Z. L.; Mai, L. Q.; Chen, J. Ultrasmall cobalt nanoparticles supported on nitrogen-doped porous carbon nanowires for hydrogen evolution from ammonia borane. *Mater. Horiz.* **2017**, *4*, 268-273.

(16) (a) Deraedt, C.; Astruc, D. "Homeopathic" Palladium Nanoparticle Catalysis of Cross Carbon-Carbon Coupling Reaction. *Acc. Chem. Res*. **2014**, *47*, 494-503. (b) Wang, D.; Deraedt, C.; Salmon, L.; Labrugère, C.; Etienne, L.; Ruiz, J.; Astruc, D. Efficient and Magnetically Recoverable "Click" PEGylated γ-Fe$_2$O$_3$-Pd Nanoparticle Catalysts for Suzuki-Miyaura, Sonogashira, and Heck Reactions with Positive Dendritic Effects. *Chem. Eur. J.* **2015**, *21*, 1508-1519. (c) Wang, D.; Deraedt, C.; Ruiz, J.; Astruc, D. Magnetic and Dendritic Catalysts. *Acc. Chem. Res*. **2015**, *48*, 1871-1880. (d) Wang, C.; Ikhlef, D.; Kahlal, S.; Saillard, J.-Y.; Astruc, D. Metal-catalyzed azide-alkyne "click" reactions: Mechanistic overview and recent trends. *Coord.*

Chem. Rev. **2016**, *316*, 1-20. (e) Liu, X.; Gregurec, D.; Irigoyen, J.; Martinez, A.; Moya, S.; Ciganda, R.; Hermange, P.; Ruiz, J.; Astruc, D. Precise localization of metal nanoparticles in dendrimer nanosnakes or inner periphery and consequences in catalysis. *Nat. Commun.* **2016**, *7*, 13152. (f) Wang, C.; Ciganda, R.; Salmon, L.; Gregurec, D.; Irigoyen, J.; Moya, S.; Ruiz, J.; Astruc, D. Highly Efficient Transition Metal Nanoparticle Catalysts in Aqueous Solutions. *Angew. Chem., Int. Ed.* **2016**, *55*, 3091-3095. (g) Ciganda, R.; Li, N.; Deraedt, C.; Gatard, S.; Zhao, P.; Salmon, L.; Hernandez, R.; Ruiz, J.; Astruc, D. Gold nanoparticles as electron reservoir redox catalysts for 4-nitrophenol reduction: a strong stereoelectronic ligand influence. *Chem. Commun.* **2014**, *50*, 10126-10129.

(17) Stanislaus, A.; Cooper, B. H. Aromatic Hydrogenation Catalysis: A Review. *Catal. Rev.: Sci. Eng.* **1994**, *36*, 75-123.

(18) Fu, F.; Wang, C.; Wang, Q.; Martinez-Villacorta, A. M.; Escobar, A.; Chong, H.; Wang, X.; Moya, S.; Salmon, L.; Fouquet, E.; Ruiz, J.; Astruc, D. Highly Selective and Sharp Volcano-type Synergistic $Ni_2Pt@ZIF-8$-Catalyzed Hydrogen Evolution from Ammonia Borane Hydrolysis. *J. Am. Chem. Soc.* **2018**, *140*, 10034-10042.

(19) Kalidindi, S. B.; Sanyal, U.; Jagirdar, B. R. Nanostructured Cu and $Cu@Cu_2O$ core shell catalysts for hydrogen generation from ammonia-borane. *Phys. Chem. Chem. Phys.* **2008**, *10*, 5870-5874.

(20) Ma, H.; Na, C. Isokinetic Temperature and Size-Controlled Activation of Ruthenium-Catalyzed Ammonia Borane Hydrolysis. *ACS Catal.* **2015**, *5*, 1726-1735.

(21) Peng, C.-Y.; Kang, L.; Cao, S.; Chen, Y.; Lin, Z.-S.; Fu, W.-S. Nanostructured Ni_2P as a Robust Catalyst for the Hydrolytic Dehydrogenation of Ammonia-Borane. *Angew. Chem. Int. Ed.* **2015**, *54*, 15725-15729.

(22) Astruc, D. *Organometallic Chemisty and Catalysis*; Springer: Heidelberg, **2007**, pp. 81-106.

TOC

Hydrogen generation

NH_3BH_3 + 4 H_2O

Dramatic Pt-Co synergy

Intradendritic triazole-NP surface Interactions accelerate catalysis

NH_4^+, $B(OH)_4^-$ + 3 H_2

PtCo NP alloy

Mechanism via oxidative additions of water O-H (rate-limiting) and ammonia borane B-H bonds on the nanoparticle (NP) surface